



Contents lists available at ScienceDirect

Brain Behavior and Immunity

journal homepage: www.elsevier.com/locate/ybrbi

GV1001 modulates neuroinflammation and improves memory and behavior through the activation of gonadotropin-releasing hormone receptors in a triple transgenic Alzheimer's disease mouse model

Hyunhee Park^{a,1}, Hyuk Sung Kwon^{a,1}, Kyu-Yong Lee^{a,1}, Ye Eun Kim^a, Jeong-Woo Son^a, Na-Young Choi^a, Eun Ji Lee^a, Myung-Hoon Han^b, Dong Woo Park^c, Sangjae Kim^{d,*}, Seong-Ho Koh^{a,e,*}

^a Department of Neurology, Hanyang University Guri Hospital, Hanyang University College of Medicine, 153, Gyeongchun-ro, Guri-si, Gyeonggi-do 11923, South Korea

^b Department of Neurosurgery, Hanyang University Guri Hospital, Hanyang University College of Medicine, 153, Gyeongchun-ro, Guri-si, Gyeonggi-do 11923, South Korea

^c Department of Radiology, Hanyang University Guri Hospital, Hanyang University College of Medicine, 153, Gyeongchun-ro, Guri-si, Gyeonggi-do 11923, South Korea

^d Teloid Inc., 3580 Wilshire Boulevard, Suite 900-31, Los Angeles, CA 90010, USA

^e Department of Translational Medicine, Hanyang University Graduate School of Biomedical Science & Engineering, Seoul 04763, South Korea

ARTICLE INFO

Keywords:

3xTg-AD mice

GV1001

Neuroinflammation

Alzheimer's disease

Gonadotropin-releasing hormone receptors

ABSTRACT

GV1001 protects neural cells from amyloid- β (A β) toxicity and other stressors in *in vitro* studies and demonstrates clinically beneficial effects in patients with moderate to severe Alzheimer's disease (AD). Here, we investigated the protective effects and mechanism of action of GV1001 in triple transgenic AD (3xTg-AD) mice. We found that GV1001 improved memory and cognition in middle- and old-aged 3xTg-AD mice. Additionally, it reduced A β oligomer and phospho-tau (Ser202 and Thr205) levels in the brain, and mitigated neuroinflammation by promoting a neuroprotective microglial and astrocyte phenotype while diminishing the neurotoxic ones. *In vitro*, GV1001 bound to gonadotropin releasing hormone receptors (GnRHRs) with high affinity. Levels of cyclic adenosine monophosphate, a direct downstream effector of activated GnRHRs, increased after GV1001 treatment. Furthermore, inhibition of GnRHRs blocked GV1001-induced effects. Thus, GV1001 might improve cognitive and memory functions of 3xTg-AD mice by suppressing neuroinflammation and reducing A β oligomers levels and phospho-tau by activating GnRHRs and their downstream signaling pathways.

1. Introduction

The number of patients with Alzheimer's disease (AD) has increased considerably in recent years, and caring for patients with AD has become a huge challenge (Jang et al., 2021; Prince et al., 2013). Senile plaques and neurofibrillary tangles (NFTs) are the most significant pathological manifestations of AD, and amyloid- β (A β) and hyperphosphorylated tau,

the major components of senile plaques and NFTs, respectively, are involved in most critical pathogenic mechanisms of AD (He et al., 2018; Nazem et al., 2015). Other mechanisms such as mitochondrial dysfunction, oxidative stress, insulin resistance, and neuroinflammation are also involved in the pathogenesis of AD. Five drugs, including tacrine and memantine, have been approved for use to improve the symptoms of AD in 1993 and 2003, respectively. However, the use of tacrine was

Abbreviations: A β , amyloid- β ; AD, Alzheimer's disease; Axl, axial; BBB, blood-brain barrier; BCS, body condition scoring; cAMP, cyclic adenosine monophosphate; CCAC, Canadian Council on Animal Care; Cor, coronal; FFE, fast field echo; FOV, field of view; GFAP, glial fibrillary acidic protein; GnRH, gonadotrophin-releasing hormone; GnRHR, gonadotrophin-releasing hormone receptor; GO, Gene Ontology; hTERT, human telomerase reverse transcriptase; IL-1 β , interleukin-1 β ; ISH, In-situ hybridization; KCL, potassium chloride; LOWESS, locally weighted scatterplot smoothing; MRI, magnetic resonance imaging; NFT, neurofibrillary tangle; NSA, number of signal averaging; NSCs, neural stem cells; SPHK1, sphingosine kinase type 1; UGT1A1, uridine diphosphate glucuronosyltransferase 1A1; WT, wild-type; 3xTg-AD, triple transgenic Alzheimer's disease.

* Corresponding author at: Department of Neurology, Hanyang University Guri Hospital, Hanyang University College of Medicine, 153, Gyeongchun-ro, Guri-si, Gyeonggi-do 11923, South Korea (S.-H. Koh).

E-mail addresses: chiron@gemvax.com (S. Kim), ksh213@hanyang.ac.kr (S.-H. Koh).

¹ Park HH, Kwon HS, and Lee KY contributed equally to this work.

<https://doi.org/10.1016/j.bbi.2023.10.021>

Received 25 June 2023; Received in revised form 22 September 2023; Accepted 22 October 2023

Available online 25 October 2023

0889-1591/© 2023 The Authors. Published by Elsevier Inc. This is an open access article under the CC BY license (<http://creativecommons.org/licenses/by/4.0/>).

discontinued in 2013 owing to its hepatotoxicity. Aducanumab and lecanemab were granted accelerated approval for the treatment of mild cognitive impairment and early dementia due to AD by the US Food and Drug Administration in June 2021 and January 2023, respectively (Larkin, 2023; Liu and Howard, 2021). Despite numerous attempts to develop new drugs, no other drugs have been approved for AD, especially for moderate to severe dementia. Therefore, there is a vast unmet medical demand for drugs to treat AD (Cummings et al., 2022; Frozza et al., 2018).

Many experts agree that the targeting of a single AD pathogenic mechanism is a major reason for the recurrent failures of clinical trials that use newly developed drugs for AD (Anderson et al., 2017; Frozza et al., 2018; Schott et al., 2019). Therefore, potential therapeutic agents should be screened for multiple effects, such as simultaneous modulation of neuroinflammation, Aβ oligomers, and phosphorylated tau (p-tau).

GV1001, originally developed as an anticancer therapeutic agent based on human telomerase reverse transcriptase (hTERT) (Relitti et al., 2020), is a 16 amino-acid peptide corresponding to a fragment of the hTERT catalytic site (Park et al., 2014). GV1001 has diverse biological functions, including antioxidant, anti-inflammatory, anti-aging, anti-apoptotic, and mitochondria-stabilizing effects (Ko et al., 2015; Park et al., 2016). We previously presented evidence indicating that GV1001 protects neural cells against Aβ and other stressors *in vitro* by mimicking the extra-telomeric function of hTERT (Park et al., 2014; Park et al., 2018; Park et al., 2016). Based on these results, we conducted a phase IIa

clinical trial using GV1001 in patients with moderate to severe AD, in which GV1001 was demonstrated to have clinically beneficial effects on cognitive function (Koh et al., 2021). However, the exact mechanisms of action of GV1001 *in vivo* remain unclear. In this study, we aimed to determine whether GV1001 can improve memory and cognition in middle- and old-aged AD mice and to investigate its mechanism of action.

2. Methods

2.1. Animals

All experiments involving animals were conducted in compliance with the Hanyang University guidelines for the care and use of laboratory animals. Our study was approved by the Institutional Animal Care and Use Committee of Hanyang University (2014-0051A). We made every effort to minimize the number of animals used and reduce animal suffering. Each animal was used only once.

Middle- and old-aged 3xTg-AD mice (B6; 129-Psen1 tm1Mpm Tg [APP^{Swe}, tauP301L] 1Lfa/Mmjax) and corresponding wild-type (WT) (B6129SF2/J) mice used in this study were obtained from the Jackson Laboratory (Bar Harbor, ME, USA).

The middle and old-aged 3xTg-AD mice were divided into groups, with 10–12 animals assigned to each group. WT mice were also used. The sex of the mice used is shown in the [Supplementary Table 1](#).

The middle-aged 3xTg-AD mice groups were classified as follows: the

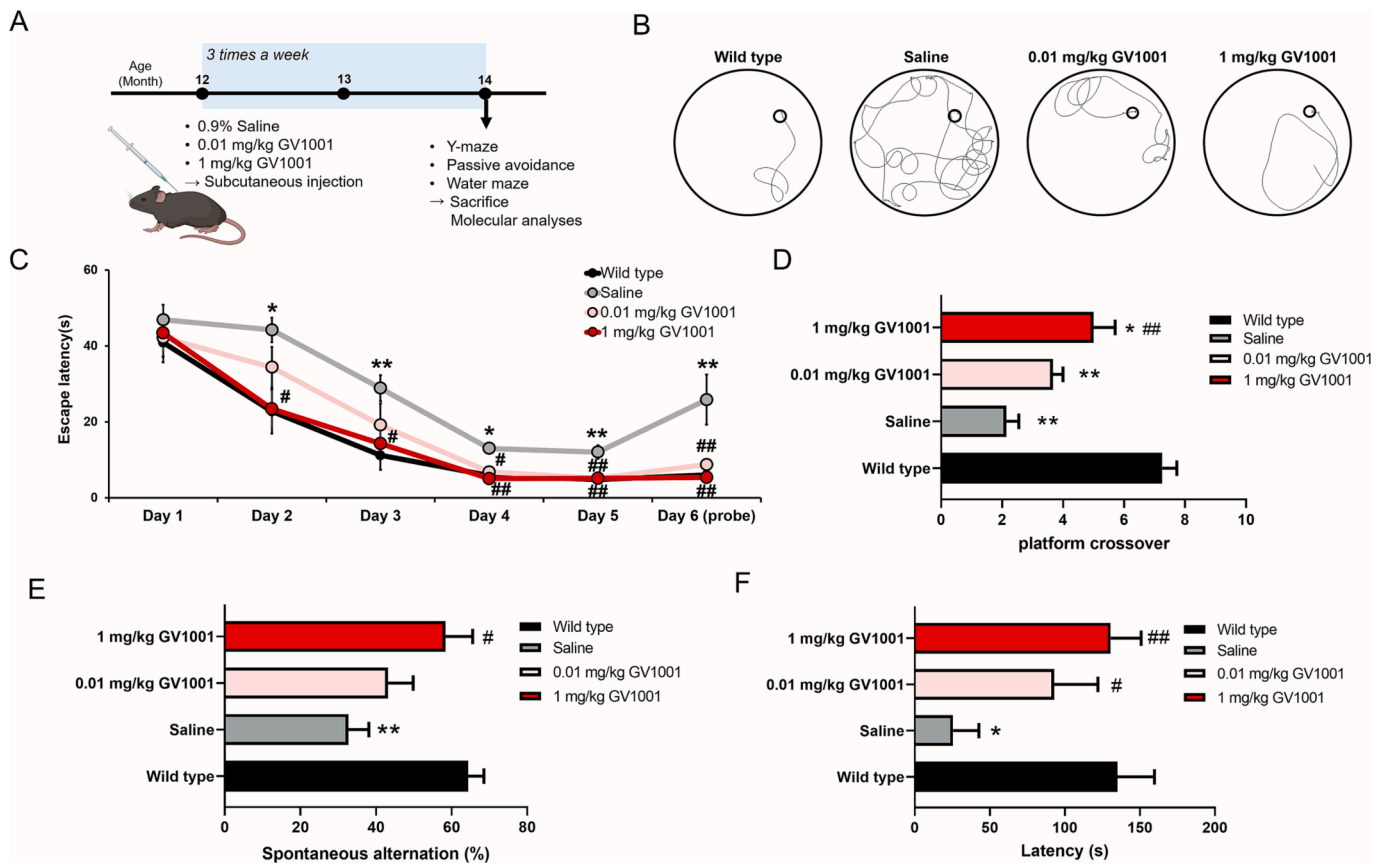


Fig. 1. Memory and neurobehavioral function of middle-aged 3xTg-AD mice after GV1001 treatment. (A) A low or high dose of GV1001 (0.01 or 1 mg/kg, respectively) or a 0.9% saline was subcutaneously injected into middle-aged (12-month-old) 3xTg-AD mice (3xTg-AD, n = 10; wild-type, n = 5; saline group, n = 10; 0.01 mg/kg GV1001 group, n = 10; 1 mg/kg GV1001 group, n = 10). The injections were administered three times a week for 2 months. (B) In the Morris water maze probe test, GV1001 administration markedly reduced the escape latency (C) and improved platform crossover (D). Mice in the 1 mg/kg GV1001 group showed a higher percentage of spontaneous alternations in the Y-maze test (E) and a longer latency of entry into the dark compartment during the passive avoidance task (F). One-way analysis of variance followed by Tukey's post-hoc analysis was used to test for significance among groups (**p* < 0.05; ***p* < 0.01 vs. wild-type; #*p* < 0.05; ##*p* < 0.01 vs. saline).

1) 0.9% saline, 2) 0.01 mg/kg GV1001, and 3) 1 mg/kg GV1001 groups (Fig. 1A). Mice in the GV1001 and saline groups were subcutaneously injected with GV1001 or an equivalent volume of saline, respectively, in a blinded manner three times a week for 2 months from the age of 12 months. Behavioral tests (passive avoidance, Y-maze, and Morris water maze tests) were then conducted to assess cognitive and memory functions.

The old-aged 3xTg-AD mice groups were classified as follows: the 1) 0.9% saline and 2) 1 mg/kg GV1001 groups (Fig. 2A). Mice in the GV1001 and saline groups were subcutaneously injected with GV1001 or an equivalent volume of saline, respectively, in a blinded manner. These treatments were administered three times a week, starting from the age of 21 months and continuing until the endpoint for sacrifice, which was identified based on the Canadian Council on Animal Care (CCAC) guidelines (<https://www.ccac.ca/en/>) (Supplementary Tables 2 and 3) (Olfert et al., 1998; Ullman-Cullere and Foltz, 1999). Because the Morris water maze experiment cannot be performed repeatedly (Cnops et al., 2022), it was conducted following the same protocol applied to middle-aged mice that received injections for a duration of 2 months. Subsequently, behavioral experiments were conducted to confirm improvements in cognitive function. However, to determine whether the drug was safe and effective in the long term, the injections and behavioral tests (Y-maze and passive avoidance task) were continued to the endpoint individually.

Each behavioral experiment was performed independently on different days. The behavioral tests results for the old-aged 3xTg-AD mice groups were evaluated using locally weighted scatterplot smoothing (LOWESS), which accounts for correlations to obtain the calibration factor.

2.2. Morris water maze test

We conducted the Morris water maze test to assess the spatial perception ability and short- and long-term memory recovery of middle- and old-aged 3xTg-AD mice after drug or vehicle administration. A cylindrical tank of 180 cm in diameter and 50–60 cm in height was filled with water (temperature, 22 ± 2 °C) to a height of 30 cm. A video camera, laboratory bench, and visual cues of various shapes, which remained constant throughout the experiment, were positioned along the perimeter of the tank. A circular platform (diameter, 12 cm) was also placed such that it was exposed 1–1.5 cm above the surface of the water. The tank was divided into the northeast, northwest, southeast, and southwest quadrants, and the platform was placed at the center of the northeast quadrant. One quadrant was consistently used as the starting position, and each trial lasted ≤ 60 s. Two months following injection, the experiment took place, precisely one week after the last day of injection. During this experiment, an acquisition phase was initiated, which involved removing the platform on day 6 (probe test) after an initial five-day training period, while simultaneously recording the route and time (upper limit of measurement: 60 s). Notably, the old-aged mice groups underwent a 'reversal phase' in which the platform positions and learning directions were reversed after a week of rest. The behaviors of all animals were recorded using a video camera, and the data were analyzed using the SMART program (Panlab, Barcelona, Spain).

2.3. Y-maze test

The Y-maze test was conducted in the old-aged 3xTg-AD mice groups (once a week until age of 25 months and once every three days after 25

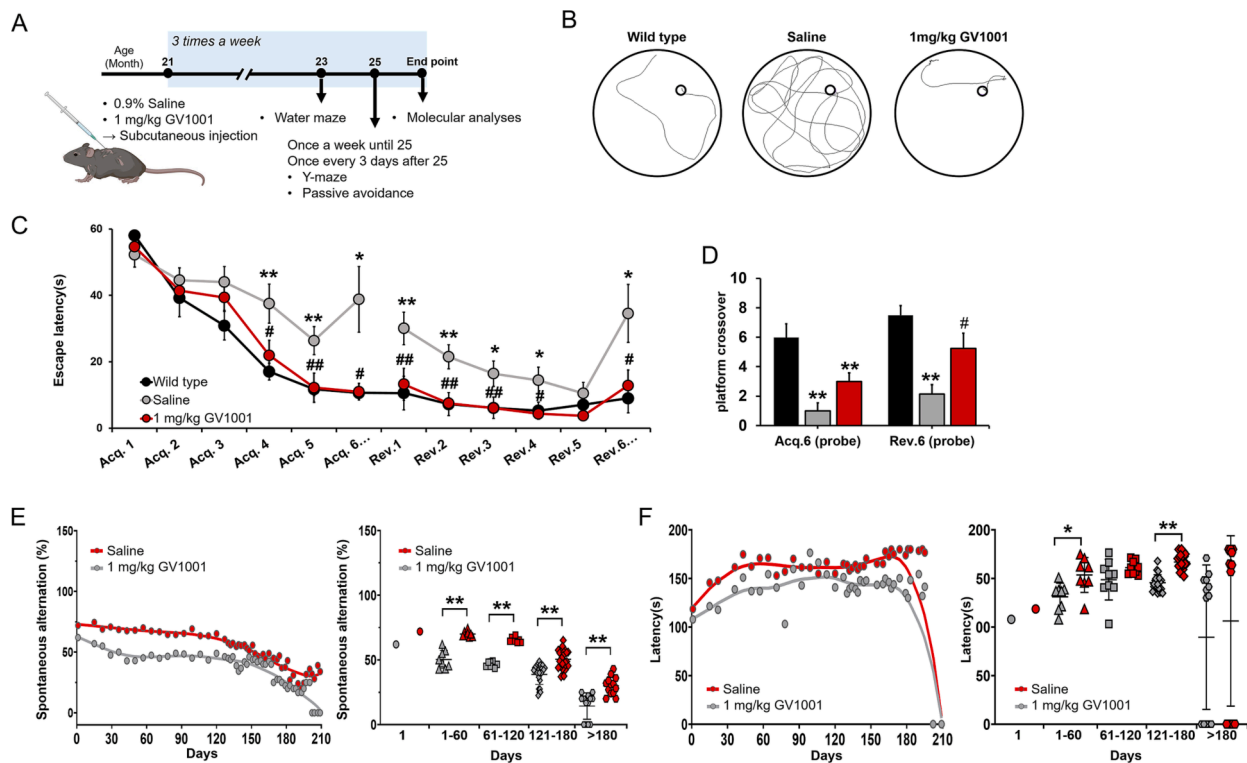


Fig. 2. Memory and neurobehavioral function of old-aged 3xTg-AD mice after GV1001 treatment. (A) A high dose of GV1001 (1 mg/kg) or a 0.9% saline was subcutaneously injected into old-aged 3xTg-AD mice from the age of 21 months. (B) The Morris water maze test was conducted, and (C) acquisition and reversal and (D) platform crossover in the two probe tests were compared among groups. All results from the Morris water maze test showed that treatment with 1 mg/kg of GV1001 markedly improved the memory and performance, (E) In the Y-maze test, GV1001 significantly improved the percentage of spontaneous alternations among the mice in the Y-maze arms. (F) In the passive avoidance task, the mice's latency to enter the dark compartment was significantly improved following treatment with 1 mg/kg of GV1001. One-way analysis of variance followed by Tukey's post-hoc analysis was used to test for significance among groups (* $p < 0.05$; ** $p < 0.01$ vs. wild-type; # $p < 0.05$; ## $p < 0.01$ vs. saline).

months) and just once in the middle-aged 3xTg-AD mice groups after the Morris water maze test to investigate whether GV1001 aided spatial perception and short-term memory recovery in old-aged 3xTg-AD mice (Hughes, 2004). The apparatus consisted of a Y-shaped maze with three arms angled at 120° to one another, designated as arms A, B, and C. The mice could move freely between the three arms; however, as mice usually prefer navigating to new locations, they tend to go into a new arm rather than returning to an already-visited arm. For each test, a mouse was placed on one arm facing the wall and allowed to move freely for 180 s. We observed the movements of each mouse and measured the percentage of spontaneous alternations by scoring the sequence of movement as follows:

$$\begin{aligned} & (\text{Number of different paths taken} / \text{total moves} - 1) \times 100\% \\ & = \text{spontaneous alternation (\%)} \end{aligned}$$

2.4. Passive avoidance test

The passive avoidance test was conducted in middle-aged 3xTg-AD mice after the conclusion of the Y-maze experiment. For old-aged mice, the test began at the age of 21 months, coinciding with the commencement of injections, and continued until the point at which the mice could be sacrificed, following the guidelines established by the CCAC for selecting an appropriate endpoint in experiments using animals for research, teaching, and testing. Accordingly, when the total score was above five or when the score for a single item was three, this endpoint was said to have been reached (Supplementary Tables 2 and 3) (Olfert et al., 1998; Ullman-Cullere and Foltz, 1999). The apparatus consisted of a lit and dark compartments connected with a door. On day 1, we placed the animal in the lit compartment; when the animal began to move, the door opened automatically and remained open for 180 s. On day 2, we followed the same procedure, except that a direct current (5 V/0.05 mA) was applied for 10 s when the mouse entered the dark compartment. On day 3, we measured the latency and frequency of the mice's entry into the dark compartment using the same procedure as used on the first day (maximum latency: 180 s).

2.5. MRI

To visualize GV1001 in the brains of the 12-month-old 3xTg-AD and 8-month-old WT mice using MRI, ferrocene carboxylic acid was conjugated to GV1001. Two-dimensional (2D) imaging with axial (Axl) fast field echo (FFE) and 2D coronal (Cor) FFE MRI were performed using a dStream Microscopy 47 mm coil set (Philips, Cambridge, MA, USA) and 3.0 T MRI device (Ingenia 3.0 T CX; Philips, Amsterdam, Netherlands). Mouse brains were scanned using the 2D Axl FFE MRI (repetition time/time echo [TR/TE] = 596 ms/16 ms, number of signal averages [NSA] = 10 ms, sense = 2, slide thickness/gap = 0.8/0 mm, matrix = 132 × 130, field of view [FOV] = 39 × 39 mm) and 2D Cor FFE MRI (TR/TE = 596/16 ms, NSA = 10 ms, sense = 2, slide thickness/gap = 0.7/0 mm, FOV = 39 × 39 mm) before the GV1001 injection. The 3xTg-AD and WT mice then received intravenous injections of 200 μL of 1 mM Fe-GV1001. After 1 h, 2D Axl FFE and 2D Cor FFE images were acquired again. Several sections of the entire brain were visualized along the dorsoventral and anteroposterior planes. All animals were sacrificed for histological examination once the MRI scans were completed.

2.6. Other analyses

We also performed various other analyses, including 1) Prussian blue staining, 2) immunofluorescence staining, 3) western blotting, 4) mRNA sequencing analysis using with Gene Ontology (GO) and signature analyses, 5) cAMP enzyme immunoassay, 6) RNA in situ hybridization, 7) Intravital imaging system, 8) cell culture, 9) GnRHR knockdown and knock-in, 10) cell viability and trypan blue staining, and 11) proteomics with protein–protein interaction networks (details provided in the

Supplementary Methods).

2.7. Statistical analysis

All data were presented as mean ± standard deviation values from independent experiments. One-way analysis of variance followed by Tukey's post-hoc comparisons was used for the statistical analyses of three or more datasets; Student's *t*-test was used for comparisons between two groups. Survival outcomes were assessed using the Kaplan–Meier estimator method and compared using the log-rank test; *p* values less than 0.05 were considered statistically significant. All statistical analyses were performed using SPSS 21.0 (SPSS Inc., Chicago, IL, USA).

3. Results

3.1. Effect of GV1001 on memory, neurobehavioral functions, and survival in middle and old-aged 3xTg-AD mice

GV1001 was injected subcutaneously into middle- and old-aged triple transgenic AD (3xTg-AD) mice according to the designated experimental schedules (Figs. 1A and 2A, respectively). Subsequently, the Morris water maze (D'Hooge and De Deyn, 2001; Morris et al., 1982), Y-maze (Kraeuter et al., 2019), and passive avoidance (Bartus et al., 1982) tests were conducted to evaluate the corresponding effects on spatial learning and memory. In the Morris water maze test, the movement of middle-aged mice in a water bath during a probe test was traced (Fig. 1B), and the results showed that mice in the 1 mg/kg GV1001 group took a significantly shorter time to reach the platform on days 2–6 than those in the saline group did (Fig. 1C). Attempts to find the hidden platform in the probe test on day 6 after five training days were also significantly increased in the 1 mg/kg GV1001 mice group (Fig. 1D). The Y-maze test results confirmed a significant improvement in spatial working memory of the treatment group, indicated by increased attempts to enter a novel arm rather than returning to the visited arm (Fig. 1E). In the passive avoidance test, the waiting time for the mice to move from the lit room to the dark room after three training days was significantly higher in the treatment group than that in the control group (Fig. 1F).

Similar results were obtained in the old-aged mice group (Fig. 2A–F). In the Morris water maze test, the movements of old-aged mice were traced in the water bath during the probe test (Fig. 2B). In the old-aged mice group, the reversal phase was performed after the acquisition phase, and the time to reach the platform was significantly shorter in the 1 mg/kg GV1001 group than that in the saline group on each day (Fig. 2C). In both probe tests (acquisition and reversal phase), attempts to find the hidden platform (number of platform cross over) were significantly increased in the treatment group compared to that in the saline group (Fig. 2D). The Y maze test confirmed a statistically significant increase in spontaneous alternation in mice treated with 1 mg/kg GV1001 compared with that in mice treated with saline from the start date to 180 days onward (Fig. 2E). Similarly, the results of the passive avoidance test indicated an overall improvement in the 1 mg/kg GV1001-treated mice; specifically, the latency tended to be higher compared to that in the saline group and was significantly increased in the 1–60 day and 121–180 day periods (Fig. 2F).

3.2. Passage of GV1001 across the blood–brain barrier (BBB) and effects of GV1001 on Aβ and p-tau levels

By assessing the presence of ferrocene carboxylic acid-conjugated GV1001 in the brain using magnetic resonance imaging (MRI) (Fig. 3A) and Prussian blue staining (Fig. 3B) as previously described (Park et al., 2018), we confirmed that GV1001 could cross the BBB in mice. GV1001 significantly reduced the levels of Aβ oligomers and p-tau in the brains of middle-aged (Fig. 3C and E) and old-aged (Fig. 3D and F)

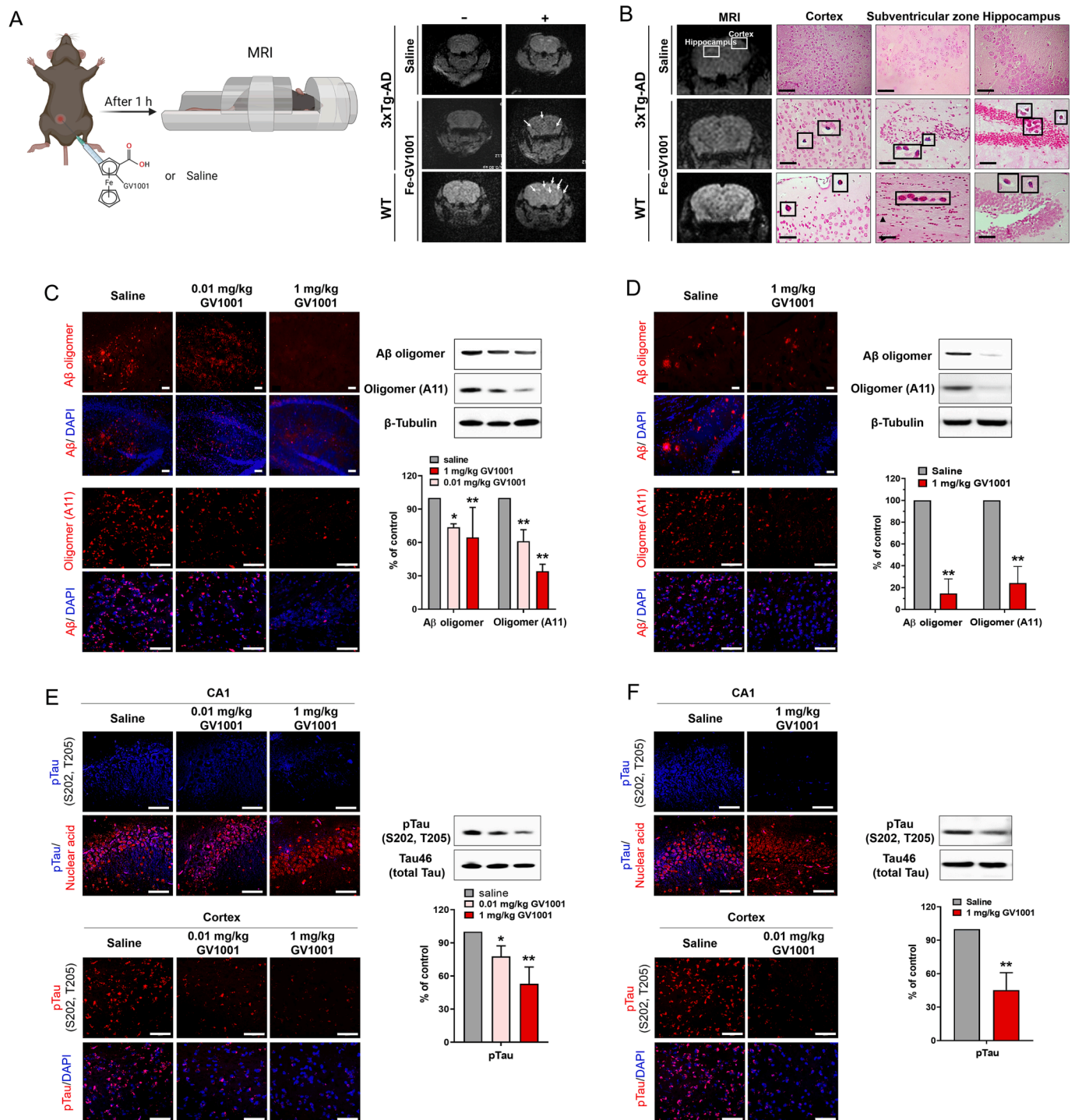


Fig. 3. Penetration of GV1001 into the brain through the blood–brain barrier and the effect of GV1001 on amyloid β (Aβ) and tau. (A and B) To confirm that GV1001 can enter the brain, 1 mg/kg of GV1001 conjugated with ferrocene carboxylic acid was subcutaneously injected into 3xTg-AD (12-month-old) and wild-type (8-month-old) mice. The presence of the conjugate was detected as dark signals in the brain on 3 T magnetic resonance images (white arrow in A and B) and Prussian blue staining images (black boxes in B). (C–F) GV1001 significantly reduced the levels of Aβ oligomers and phosphorylated tau in the brains of middle-aged (C and E) and old-aged (D and F) 3xTg-AD mice, as confirmed using immunohistochemical and western blotting analyses. Statistical analysis was performed using one-way analysis of variance followed by Tukey’s post-hoc test for multiple comparisons and unpaired Student’s *t*-tests for individual comparisons (**p* < 0.05; ***p* < 0.01 vs. saline). *F*-value = 6.872 (C; Aβ oligomers), 122.68 (C; A11) and 61.283 (E), *t*-value = 14.320 (D; Aβ oligomers), 12.358 (D; A11) and 9.936 (F). Scale bar = 50 μm (B, C [A11], E, and F) or 100 μm (C [Aβ oligomer] and D).

3xTg-AD mice as confirmed using immunohistochemical and western blotting analyses. Specifically, our results showed that both 0.01 mg/kg and 1 mg/kg of GV1001 significantly reduced Aβ oligomer levels, as analyzed using two different types of primary antibodies (rabbit anti-β-amyloid [oligomer, AB9234] and rabbit anti-oligomer [A11,

AHB0052]) to obtain more definite results, and p-tau (S202 and T205) levels in middle-aged AD mice (Fig. 3C and E, respectively) in a concentration-dependent manner. Similarly, old-aged AD mice treated with 1 mg/kg of GV1001 had a vast reduction in the levels of Aβ oligomers and p-tau (S202 and T205) compared to those of mice in the

saline group (Fig. 3D and F, respectively). However, GV1001 did not reduce the levels of tau46 (total tau) in either middle- or old-aged AD mice; thus, the ratio of p-tau and total tau after GV1001 treatment was much lower in these mice (Fig. 3E and F, respectively).

3.3. Effect of GV1001 on neuroinflammation in the brain

In terms of neuroinflammation in the brain, GV1001 reduced the number of reactive glial fibrillary acidic protein (GFAP)-positive cells in the brains of both middle- and old-aged mice (Fig. 4A and B, respectively).

The expression of uridine diphosphate glucuronosyltransferase

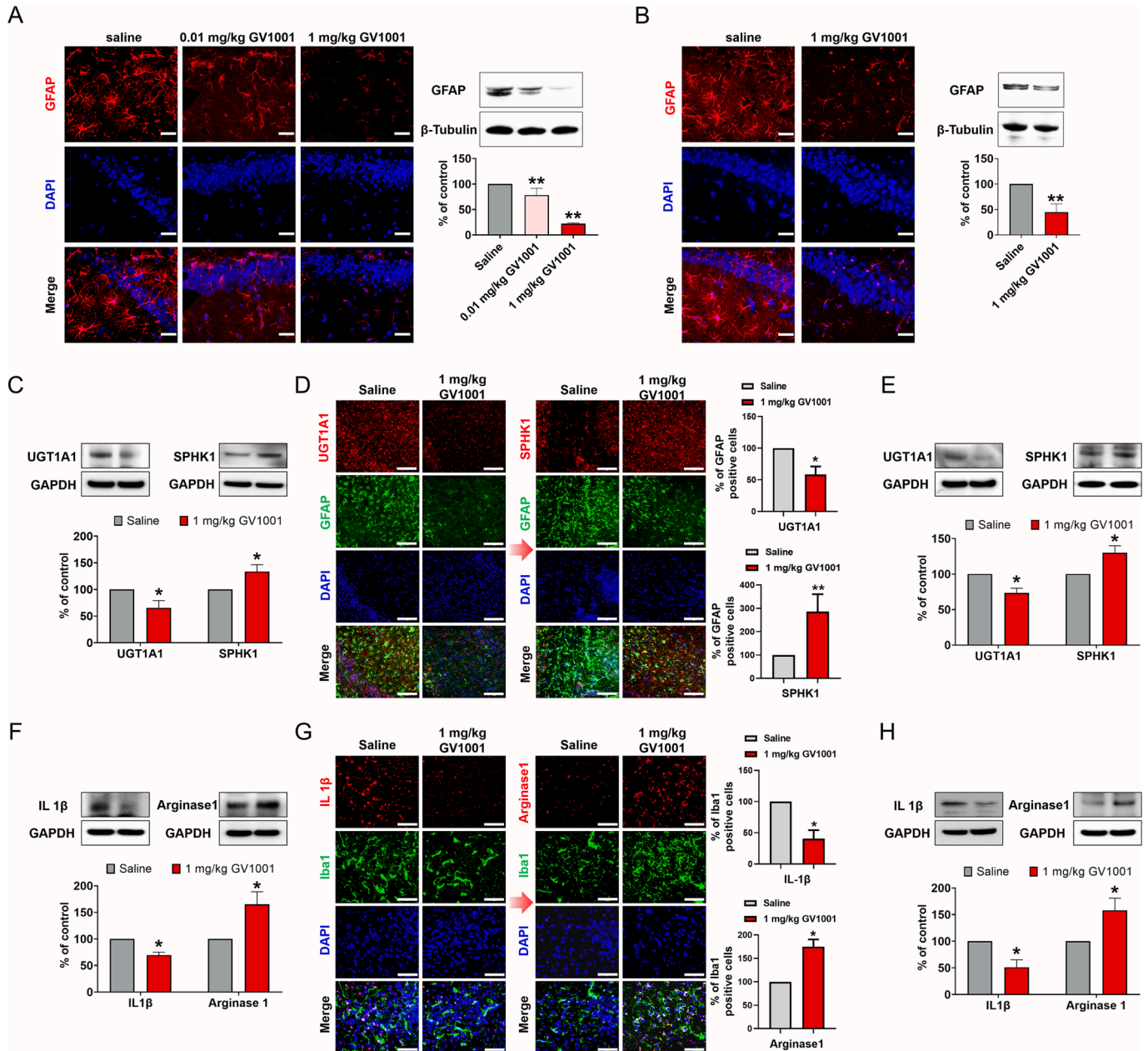


Fig. 4. Effect of GV1001 on neuroinflammation in the brain. Immunohistochemical staining and western blotting analyses showed significant decrease in the expression of glial fibrillary acidic protein (GFAP) in middle- and old-aged 3xTg-AD mice (A and B, respectively) after treatment with GV1001. GV1001 significantly reduced the expression of uridine diphosphate glucuronosyltransferase family 1 number A1 (UGT1A1) and increased sphingosine kinase 1 (SPHK1) expression, which might indicate that GV1001 reduced the number of neurotoxic astrocytes and increased the number of neuroprotective astrocytes in middle- and old-aged 3xTg-AD mouse brains (C, D and E, respectively). Additionally, Treatment with GV1001 reduced interleukin (IL)-1 β expression and increased arginase 1 expression in the middle and old-aged 3xTg-AD mice brain (F, G and H, respectively). This indicates that GV1001 reduces the number of neurotoxic microglia and increases the number of neuroprotective microglia. Statistical analysis was performed using one-way analysis of variance followed with Tukey's post-hoc test for multiple comparisons and the unpaired Student's *t*-test for two individual comparisons (**p* < 0.05; ***p* < 0.01 vs. saline). F-value = 130.689 (A), *t*-value = 7.768 (B), 4.352 (C; UGT1A1), -4.559 (C; SPHK1), 5.673 (D; UGT1A1) -5.558 (C; SPHK1), 6.989 (E; UGT1A1), -5.263 (E; SPHK1), 9.553 (F; IL-1 β), -4.768 (F; Arginase1), 7.529 (G; IL-1 β), -10.928 (G; Arginase1) and 5.972 (H; IL-1 β), -4.423 (H; Arginase1). Scale bar = 30 μ m (A, B, and D) or 50 μ m (G). Data are expressed as the mean (% of control) \pm standard deviation values from three to five independent experiments. The treatment groups were compared using two-way analysis of variance followed with Tukey's post-hoc test. (**p* < 0.05; ***p* < 0.01 vs. the control group).

family 1 number A1 (UGT1A1), a neurotoxic astrocyte marker, and sphingosine kinase 1 (SPHK1), a neuroprotective astrocyte marker, was measured in middle-aged (Fig. 4C) and old-aged (Fig. 4D and E) 3xTg-AD mice following GV1001 treatment to evaluate the effects of GV1001 on the neurotoxic and neuroprotective phenotypes of astrocytes. GV1001 significantly reduced UGT1A1 expression and increased SPHK1 expression, indicating that GV1001 may reduce the number of neurotoxic astrocytes and increase the number of neuroprotective astrocytes in middle- and old-aged 3xTg-AD mouse brains.

To evaluate the effects of A β and GV1001 on the expression of neurotoxic and neuroprotective markers of microglial phenotypes in the brains of the middle- (Fig. 4F) and old-aged (Fig. 4G and H) 3xTg-AD mice, the expression of interleukin (IL)-1 β , a marker of neurotoxic microglia, and arginase 1, a marker of neuroprotective microglia, was also measured. Treatment with GV1001 reduced IL-1 β expression and increased arginase 1 expression in the middle- and old-aged 3xTg-AD mice brains, indicating that GV1001 might reduce the number of neurotoxic phenotype microglia while concurrently promoting the population of neuroprotective microglia.

Functional enrichment analysis results for significantly upregulated or downregulated mRNAs in the hippocampus of 3xTg-AD mice after GV1001 treatment were visualized using the ClueGO (Fig. 5A and Supplementary Fig. 1A). Interestingly, the GO analysis results included several relevant terms related to critical pathways and functions such as “microglial cell activation,” “positive response to acute inflammation response,” “immune response,” “oxidative stress-induced neuronal death,” “amyloid beta formation,” and “long-term memory.”

Kyoto EncycloGenomes (KEGG) pathway analysis revealed that cyclic adenosine monophosphate (cAMP) signaling pathway was one of the most strongly affected pathways by the GV1001 (Fig. 5B), and we also confirmed that GV1001 treatment markedly increased the cAMP level (Fig. 5C) in 3xTg-AD mouse brains.

In addition, proteomic analysis confirmed that the effects of GV1001 were mediated through its effects on diverse intracellular signaling pathways (Supplementary Fig. 1B and 1C). The accompanying Venn diagram illustrates the functional classification of the selected proteins closely related to AD, inflammatory responses, and aging (Supplementary Fig. 1B; Supplementary Table 4). These proteins included ATP

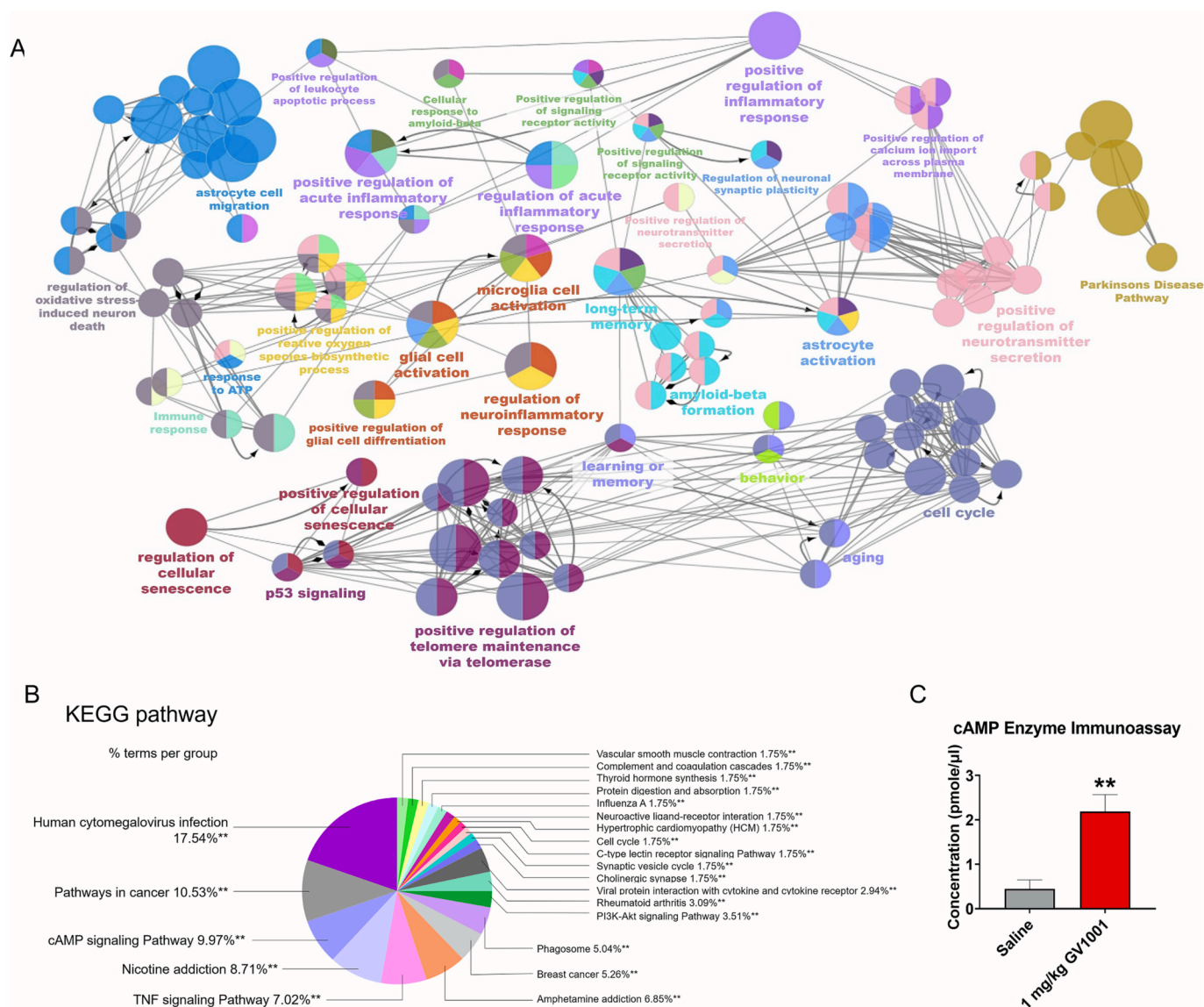


Fig. 5. ClueGo and KEGG pathway analyses. ClueGO (A) and KEGG pathway (B) analyses were used to visualize the functional enrichment results of significantly up- and down-regulated mRNAs associated with inflammation in the 3xTg-AD mice treated with GV1001 compared to those of mice treated with saline, using the Gene Ontology (GO) functional network. (C) The KEGG pathway analysis showed that the cyclic adenosine monophosphate (cAMP) signaling pathway is one of those most affected by GV1001 (** $p < 0.01$ vs. saline). Therefore, we confirmed that cAMP level was significantly increased in the of 3xTg AD mice brain treated with GV1001.

synthase subunit alpha (Goldberg et al., 2018; Misrani et al., 2021), cofilin-1 (Alhadidi and Shah, 2018; Hadas et al., 2012; Wang et al., 2020), nucleophosmin (Haghani et al., 2020), alpha-enolase isoform X1 (Butterfield and Lange, 2009; Choi et al., 2015), 60 kDa heat shock protein (Grundtman et al., 2011), and phosphatidylethanolamine-binding protein 1 (Kim et al., 2019b).

3.4. Mechanism of action of GV1001 through the activation of gonadotropin-releasing hormone receptors (GnRHRs)

To see if GV1001 could bind to the GnRHRs of brain cells and activate them as a major action mechanism, we first conducted dual in situ hybridization (ISH) for GnRHRs, GFAP, and allograft inflammatory factor 1 (AIF1)/ionized calcium-binding adapter molecule 1 (IBA1). As a result, GnRHR expression was detected in astrocytes expressing GFAP (Fig. 6A and B and Supplementary Fig. 2C and G) and microglia expressing IBA1 (Fig. 6E and F and Supplementary Fig. 2D and H) within the pituitary gland and hippocampus of both human and mice brain tissues. These findings confirmed the expression of GnRHRs in astrocytes and microglia across both human and mouse brain tissues.

To confirm the affinity between GV1001 and GnRHRs, an intravital imaging analysis was performed. To visualize the colocalization of fluorescein 5(6)-isothiocyanate (FITC)-labeled GV1001-IBA1-GnRH receptors and FITC-labeled GV1001-GFAP-GnRH receptors in the bregma regions of the brain tissues, repetitive intravital imaging was performed at the same locations using thinned skull or cranial window preparations over 24 and 48 h (Supplementary Fig. 4 and Supplementary Videos 1–4). We confirmed that 1 mM FITC-labeled GV1001 co-localized with GnRHRs in the astrocytes (Fig. 6C and Supplementary Fig. 4A and B) and microglia (Fig. 6G and Supplementary Fig. 4C and D) of the 3xTg-AD mouse brains through three-dimensional reconstruction using IVIM-Studio.

Our results indicated that GV1001 significantly bound to GnRHRs with high affinity in cultured human astrocytes (Fig. 6D), mouse astrocytes (Supplementary Fig. 5C), and mouse microglia (Fig. 6H and Supplementary Fig. 5D). The viability of mouse astrocytes and microglia was reduced with A β treatment, but restored after treatment with 1 nM leuprorelin (a GnRHR agonist) or GV1001 (Fig. 6I and J, respectively). However, the effect of GV1001 was completely blocked upon treatment with 100 nM degarelix or siRNA; both are specific GnRHR antagonists (Fig. 6I and J), suggesting that GnRHRs played critical roles in the protective effects of GV1001.

Finally, we demonstrated that GV1001 markedly shifted the phenotypes of mouse astrocytes (Fig. 7A) as well as mouse microglia (Fig. 7B) from neurotoxic to neuroprotective. All effects of GV1001 on astrocytes and microglia (Fig. 7A and B, respectively) were blocked by GnRHR knockdown using degarelix or siRNA treatment (Supplementary Fig. 7). These findings further indicate that GnRHR activation is a major component of the mechanism of action of GV1001.

4. Discussion

In this study, we demonstrated that GV1001 could restore memory and cognitive functions in middle- and old-aged transgenic AD mice (Figs. 1 and 2). Furthermore, these improvements appeared to be mediated by multiple protective effects of GV1001 against several pathogenic mechanisms of AD *in vivo* (Figs. 3–5). Specifically, GV1001 reduced the levels of A β oligomers and p-tau, reduced neuroinflammation-related intracellular signaling, induced a shift in the phenotypes of astrocytes and microglia from neurotoxic to neuroprotective, and activated downstream signaling pathways through binding to GnRHRs (Figs. 6–7).

Considering that drugs affecting a single molecular target have failed to show any beneficial effects against AD in several clinical trials (Anderson et al., 2017; Frozza et al., 2018; Schott et al., 2019) and that multiple mechanisms, such as amyloid deposition, NFT formation,

neuroinflammation, impaired hypothalamic function, and metabolic derangement, are involved in the pathogenesis of AD (Frozza et al., 2018), drugs that simultaneously target multiple processes might be the best solution for AD treatment. However, designing new chemical drugs with multiple action mechanisms is challenging. GV1001 is a 16 amino-acid peptide that mimics the active catalytic site of hTERT, and previous studies have confirmed that GV1001 simultaneously affects multiple cellular targets (Ko et al., 2015; Park et al., 2014; Park et al., 2018; Park et al., 2016). Based on these results, we conducted a phase IIa clinical trial in which GV1001 was used for the treatment of AD patients with moderate to severe dementia and confirmed that, compared to those in the placebo, GV1001 significantly improved the AD patient's cognitive function (Koh et al., 2021). However, no information regarding the exact mechanisms of action of GV1001 in the brain is available until the present study.

The ability of new drugs for AD to cross the BBB is important to demonstrate their efficacy (Pardridge, 2020), more so because the inability to cross the BBB is considered a possible reason for several drugs failing to be effective *in vivo*, although they had beneficial effects *in vitro* (Paris et al., 2011). To demonstrate the penetration of GV1001 through the BBB, we conjugated GV1001 to ferrocene carboxylic acid and injected it into mice. The presence of ferrocene carboxylic acid-conjugated GV1001 in the brain was detected using both MRI and Prussian blue staining (Fig. 3A and B), proving that GV1001 can enter the brain by crossing the BBB.

A β pathology and the presence of NFTs composed of hyperphosphorylated tau are considered as the hallmarks of AD (Kwon and Koh, 2020). Neuroinflammation is also related to the pathogenesis of AD and may contribute its progression (Brosseron et al., 2014; Kwon and Koh, 2020). Both microglia and astrocytes, which are neuroinflammation-related glial cells, are activated by the lesions present in the AD brain. In the early stages, the microglia surrounding A β deposits generally exhibit neuroprotective phenotypes; however, with sustained inflammatory responses, microglia switch their function and promote AD pathogenesis (Tang and Le, 2016). Astrocytes also alter their morphology and may function differently during AD progression (Carter et al., 2019).

In this study, we found that GV1001 increased the expression of neuroprotective phenotypes markers of microglia (arginase 1) and astrocytes (SPHK1) (Fig. 4) and reduced the expression of neurotoxic phenotypes markers of microglia (IL-1 β) and astrocytes (uridine diphosphate glucuronosyltransferase 1A1 [UGT1A1]) (Fig. 4). We further validated these changes by quantifying GFAP-positive and IBA1-positive cells that also exhibited positivity for these biomarkers (Fig. 4D and G). However, microglia and astrocytes are known to have multiple reactive phenotypes, and their functions are complex. Therefore, it may not be straightforward to categorize them solely based on the expression of specific biomarkers (Kwon and Koh, 2020). Additionally, our study revealed that GV1001 treatment reduced the number of reactive GFAP-positive cells (Fig. 4A and B). Notably, GFAP expression is a recognized hallmark of activation in astrocytes (Oksanen et al., 2019). Recent research has also highlighted the significance of astrocyte reactivity, as indicated by plasma GFAP levels, in influencing the effects of A β on tau pathology (Bellaver et al., 2023). Therefore, the diverse effects of GV1001 against neuroinflammation demonstrated in the current study may be attributed to the degradation of A β and tau pathology (Fig. 3) (Asai et al., 2015; Takata et al., 2010).

Although we confirmed that GV1001 could enter the brain and had beneficial effects on the 3xTg AD mice brain, similar to other peptides, identifying the predominant *in vivo* mode of action of GV1001 was challenging (Di, 2015; Lau and Dunn, 2018). A previous study that used docking prediction suggested that GV1001 binds to the GnRHR with high affinity (Kim et al., 2019a), which led us to hypothesize that GV1001 could bind to GnRHR and activate GnRHR-mediated signaling in the brain.

Initially, we confirmed the expression of GnRHRs in astrocytes and

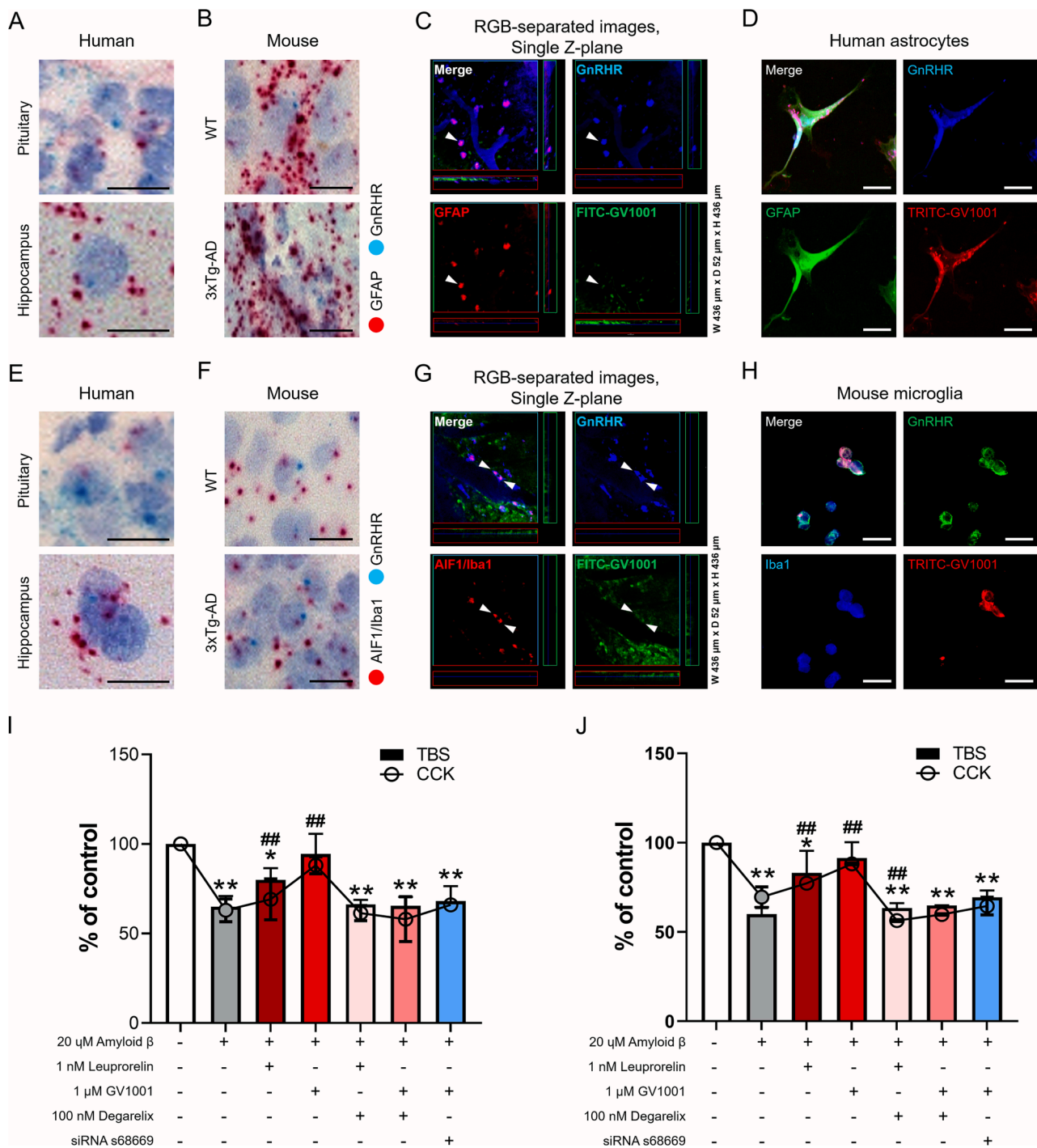


Fig. 6. The role of gonadotropin-releasing hormone receptors in GV1001-induced effects. (A–H) Binding between GV1001 and gonadotropin-releasing hormone receptors (GnRHRs) was investigated to determine the mode of action of GV1001. (A–D) Dual-probe in situ hybridization labeling of the GnRHRs with probes to (A and B) astrocytes and microglia in human brain (pituitary and hippocampus) and (C and D) mice brain (WT and 3xTg-AD) tissue samples. GFAP and AIF1 probes are labeled in red, while GnRHR probes are labeled in blue. (E and F) Intravital imaging analysis confirmed that 1 mM fluorescein 5(6)-isothiocyanate (FITC)-labeled GV1001 was co-localized with GnRHRs in (white arrow in E and F) astrocytes and microglia within the brains of 3xTg-AD mice. (G and H) Immunohistochemical analysis confirmed the expression of GnRHRs in cultured (G) human astrocytes and (H) mouse microglia. Furthermore, tetramethylrhodamine (TRITC)-conjugated GV1001 was highly co-localized with GnRHRs in human astrocytes and mouse microglia. β treatment reduced the viability of mouse astrocytes and microglia, which was restored by the treatment with GnRHR agonist leuprorelin (1 nm) and to an even greater extent by GV1001 (I and J, respectively). However, the effect of leuprorelin and GV1001 was completely blocked upon treatment with 100 nM degarelix or GnRHR-specific siRNA s68668 or siRNA s68669, which function as specific GnRHR antagonists (I and J), suggesting that GnRHRs played critical roles in the protective effects of GV1001. Statistical analyses were performed using the one-way analysis of variance (ANOVA) followed with Tukey’s post-hoc test for multiple comparisons. Scale bar = 50 μ m (A–D, G and H) or W 436 μ m \times D 52 μ m \times H 436 μ m (E and F). Data (I and J) are expressed as the mean (% of control) \pm standard deviation values from three to five independent experiments. The treatment groups were compared using Tukey’s post-hoc test after two-way ANOVA. (* p < 0.05, ** p < 0.01 vs. the control group; # p < 0.05, ## p < 0.01 vs. samples treated only with 20 μ M $A\beta_{25-35}$). F-value = 13.368 (I; TBS), 13,368 (I; CCK), 35.585 (J; TBS), 149.151 (J; CCK).

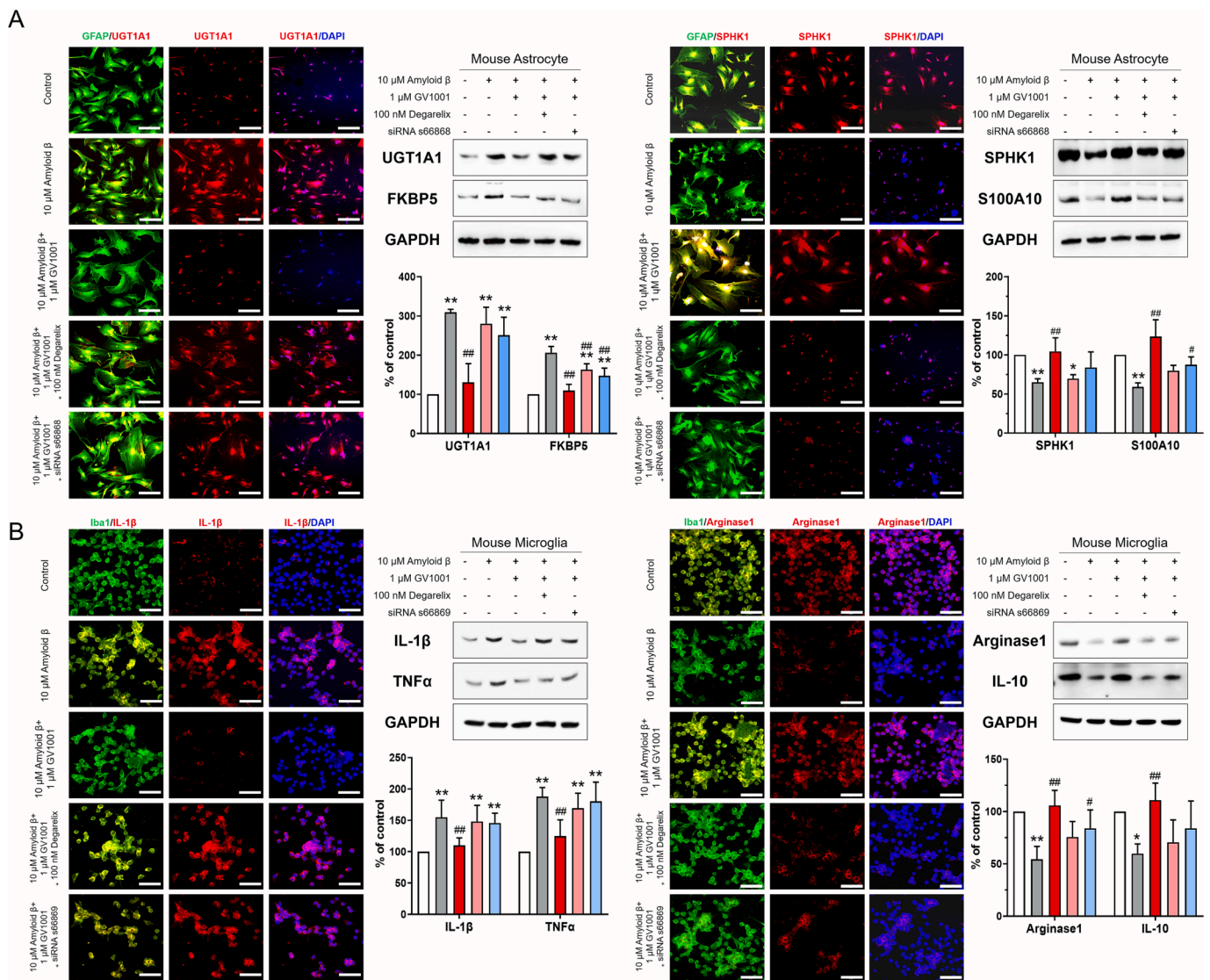


Fig. 7. The effects of GV1001 on astrocytes and microglia. (A and B) Treatment with 1 μM GV1001 reduced the expression of UGT1A1 and FK506-binding protein 5 (FKBP5), which are markers of neurotoxic astrocytes, and increased the expression of SPHK1 and S100 calcium-binding protein A10 (S100A10), which are markers of neuroprotective astrocytes, in mouse astrocytes (A). Treatment with 1 μM GV1001 reduced the expression of IL-1β and tumor necrosis factor α (TNFα), which are the markers of neurotoxic microglia, and increased the expression of arginase 1 and IL-10, which are the markers of neuroprotective microglia, in mouse microglia (B). All the effects of GV1001 were blocked by treatment with 100 nM degarelix, a GnRH antagonist, and siRNA s66868 and siRNA s66869, which induced GnRH knockdown in mouse astrocytes and microglia (A and B, respectively). These findings indicated that GnRHs played a critical role in the mechanism of action of GV1001 [F-value = (A; UGT1A1), 32.993 (A; FKBP5), 8.383 (A; SPHK1), 17.968 (A; S100A10), 8.756 (B; IL-1β), 15.334 (B; TNFα), 11.932 (B; Arginase1), 7.324 (B; IL-10)]. Data are expressed as the mean (% of control) ± standard deviation values from three to five independent experiments. The treatment groups were compared using Tukey’s post-hoc test after two-way ANOVA. (**p* < 0.05, ***p* < 0.01 vs. the control group; #*p* < 0.05, ##*p* < 0.01 vs. astrocytes treated only with 20 μM Aβ₂₅₋₃₅).

microglia in human and mouse brains (Fig. 5A, B, E, and F; Supplementary Fig. 2C, D, G, and H), consistent with previous reports (Wang et al., 2023; Xu et al., 2023). Additionally, we confirmed that GV1001 co-localized with GnRHs in astrocytes and microglia using a three-dimensional reconstruction process in IVIM-studio (Fig. 6C and G, Supplementary Fig. 4A–D, and Supplementary video files). Furthermore, an enzyme immunoassay confirmed that GV1001 significantly increased cAMP levels in the brains of 3xTg mice (Fig. 5C).

The intracellular level of cAMP, a direct downstream effector of GnRH, increases when GnRH is activated, and an increase in cAMP levels in the 3xTg AD mice brain after GV1001 treatment was observed. Therefore, we hypothesized that GV1001 binds to GnRH and further activates downstream signaling pathways, as shown by its ability to increase the concentration of cAMP. To confirm this hypothesis, we used a diverse set of *in vitro* experiments and found that i) GV1001 and

GnRH were highly co-localized (Fig. 6E, G, F, H), ii) several signaling proteins downstream of GnRH were activated after GV1001 treatment (Fig. 5B), and iii) GnRH knockdown blocked all the beneficial effects of GV1001 (Figs. 6 and 7), suggesting that GV1001 activated GnRH and that this activation was one of the vital mechanisms of action of GV1001. Although the cells used in this study are totally different from the cells in the brain, these findings were partially supported by a previous study which reported that GnRH mediated the activation of the Gsa-cAMP pathway by GV1001 in prostate cancer cells (Kim et al., 2021; Kim et al., 2019a). Moreover, GnRH activation contributes to axonal and dendritic growth in the hippocampus and cortex (Prange-Kiel et al., 2008; Skinner et al., 1995), neuroprotection, induction of neuroregeneration (Quintanar and Salinas, 2008), and improvement of working memory and executive functions in young pre-menopausal women (Grigороva et al., 2006) as well as extinction memory in rats

(Maeng et al., 2017). Additionally, gonadotropin-releasing hormone (GnRH), which activates the GnRH receptor (GnRHr), is known to have protective effect against Aβ toxicity (Marbouti et al., 2020), and GnRH agonists might reduce AD-related mortality risk and aging-related health problems (D'Amico et al., 2010; Zhang et al., 2013). cAMP, a direct downstream effector of GnRHr, promotes the conversion of microglial phenotypes from neurotoxic to neuroprotective (Ghosh et al., 2016). Considering our present findings and those of previous studies, we propose that GnRHr activation is an important mechanism of action of GV1001 and contributes to the inhibition of the pathogenic mechanisms of AD (Fig. 8).

Our previous studies have also shown that GV1001 has extra-telomeric effects on hTERT as well as antioxidant activity (Park et al., 2014; Park et al., 2016). Another study showed that telomerase reverse transcriptase protects hippocampal neurons from Aβ toxicity by enhancing the expression of genes involved in the neuronal survival and plasticity (Baruch-Eliyahu et al., 2019). These results suggest that, in addition to GnRHr activation, the extra-telomeric function of GV1001 could also contribute to its mechanism of action against AD.

The beneficial *in vitro* and *in vivo* effects of GV1001 motivated us to perform a phase IIa clinical trial, in which patients with AD and moderate to severe dementia were subcutaneously injected with 0.56 or 1.12 mg of GV1001 (Koh et al., 2021), and patients treated with 1.12 mg of GV1001 showed significant improvements in cognitive function. These positive results from the clinical trial are consistent with the *in vivo* results of the current study, and we believe that the ability of GV1001 to activate GnRHr and regulate neuroinflammation may have contributed to its beneficial effects.

Nevertheless, the present study has certain limitations. First, only 3xTg AD mice were used as an AD model. However, although there are

several different types of AD mouse models, the 3xTg AD mice (B6; 129-Psen1 tm1Mpm Tg [APPswe, tauP301L] 1Lfa/Mmjax), the model we used in the present study, are well-known to simultaneously demonstrate pathologies associated with both Aβ and tau in the brain, which is similar to the pathologies in the brains of patients with AD than that of other AD mouse models (for example, Aβ only in the 5xTg mice) (Javonillo et al., 2021; Oakley et al., 2006). By using this model rather than other AD mouse models, we could assess the effects of GV1001 on amyloidopathy and tauopathy in the brain at the same time, which might be more similar to its mechanisms of action in the brain of patients with AD. In addition, although the sex ratios of the mice were balanced, we did not initially plan to analyze each detailed experiment separately according to sex. Previous research has suggested that Aβ pathology is reported to occur and progress faster in female 3xTg-AD mice, even though significant behavioral differences between sexes may not be apparent (Dennison et al., 2021). Therefore, providing results that consider the distinctions between male and female mice could offer valuable insights. We also conducted supplementary experiments with a limited number of mice (n = 3 in each group), observing that the effect of GV1001 on reducing p-tau (S202, T205) and amyloid oligomers was not significantly different between sexes (data not shown).

In conclusion, the present study confirmed that GV1001 has multiple effects that significantly ameliorate AD pathology and improve memory and cognitive functions through the activation of GnRHr in AD model mice. Considering these results, GV1001 could be used in further clinical trials on AD treatment, and GnRHr activation might be another potential therapeutic strategy for AD treatment.

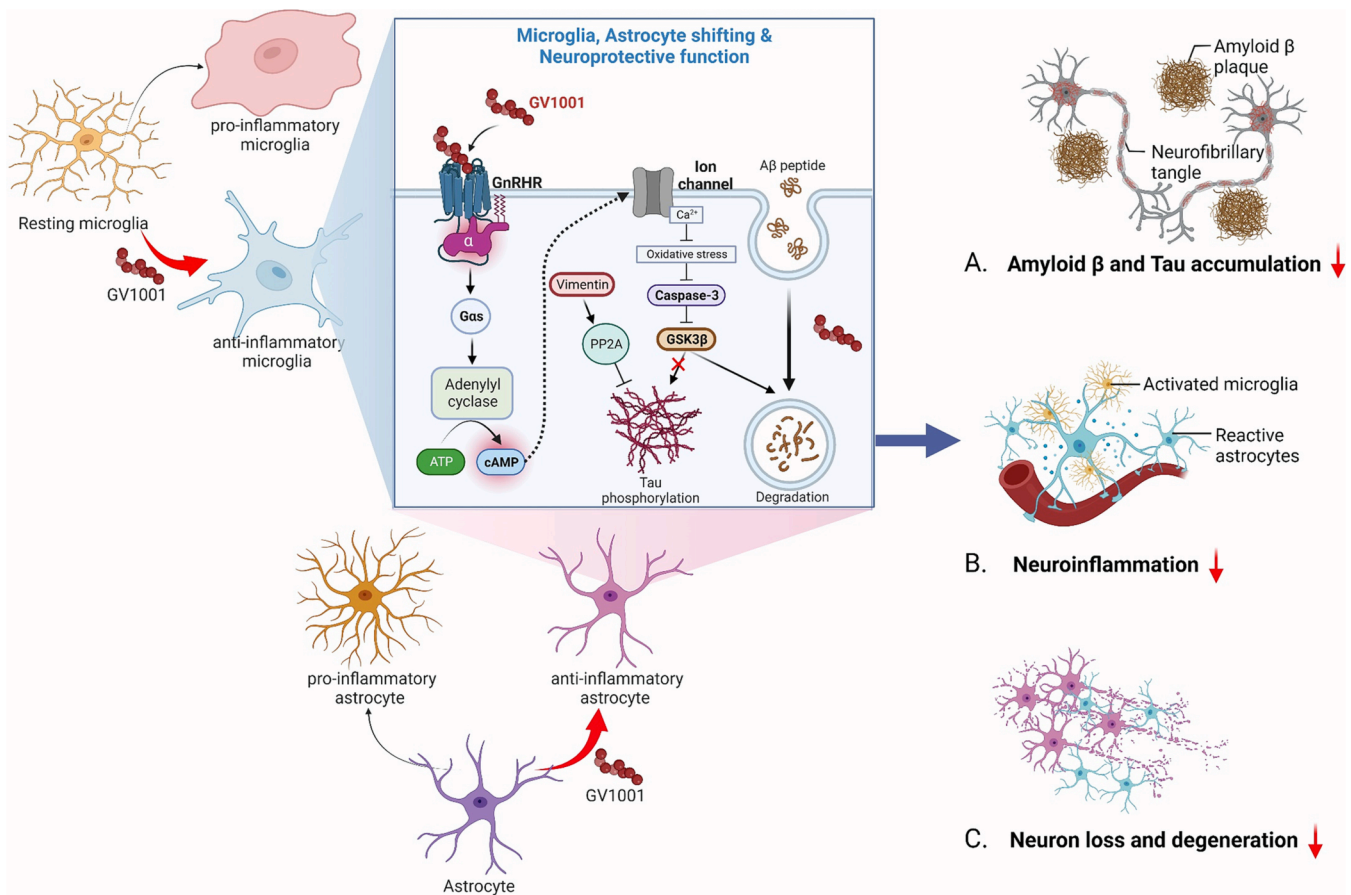


Fig. 8. Summary of the effects of GV1001 on Alzheimer's disease. GV1001 binds to GnRHr and activates downstream signaling pathways, increasing cAMP levels. This pathway might affect the degradation of Aβ peptides, reduction of p-tau, modulation of neuroinflammation (i.e., reducing pro-inflammatory and increasing anti-inflammatory microglia and astrocytes), and suppression of neuronal loss.

Author contributions

H.H.P., Y.E.K., J.W.S., N.Y.C., and S.H.K. prepared the reagents, performed the experiments, and analyzed the data. H.S.K., M.M.H., E.J.L., and D.W.P. analyzed the data and supervised the study. S.K., and S.H.K. synthesized GV1001 and Fe-GV1001. H.H.P., H.S.K., and K.Y.L. wrote the original draft. S.K., and S.H.K. conceptualized the study and revised the manuscript. H.H.P., H.S.K., and K.Y.L. contributed equally to the study. All authors have read and approved the final manuscript.

Declaration of Competing Interest

The authors declare the following financial interests/personal relationships which may be considered as potential competing interests: KSJ is an employer of GemVax & Kael Co., Ltd. and holds equity in the company. Other authors declare no competing interests.

Data availability

Data will be made available on request.

Acknowledgments

None.

Funding

This research was supported by a grant of the Korea Dementia Research Project through the Korea Dementia Research Center (KDRC), funded by the Ministry of Health & Welfare and Ministry of Science and ICT, Republic of Korea (grant numbers: HI20C0253, HU21C0113, and HU21C0007), the Medical Research Center (grant number: 2017R1A5A2015395), the National Research Foundation of Korea (grant number: NRF-2022R1A2C1092835), and GemVax & Kael Co., Ltd.

Consent for publication

All authors read and approved the final manuscript.

Ethics approval and consent to participate

All studies involving animals were performed in accordance with the Hanyang University guidelines, and the study was approved by the Institutional Animal Care and Use Committee of Hanyang University.

Appendix A. Supplementary data

Supplementary data to this article can be found online at <https://doi.org/10.1016/j.bbi.2023.10.021>.

References

- Alhadidi, Q., Shah, Z.A., 2018. Cofilin mediates LPS-induced microglial cell activation and associated neurotoxicity through activation of NF- κ B and JAK-STAT pathway. *Mol. Neurobiol.* 55, 1676–1691.
- Anderson, R.M., Hadjichrysanthou, C., Evans, S., Wong, M.M., 2017. Why do so many clinical trials of therapies for Alzheimer's disease fail? *Lancet* 390, 2327–2329.
- Asai, H., Ikezu, S., Tsunoda, S., Medalla, M., Luebke, J., Haydar, T., Wolozin, B., Butovsky, O., Kügler, S., Ikezu, T., 2015. Depletion of microglia and inhibition of exosome synthesis halt tau propagation. *Nat. Neurosci.* 18, 1584–1593.
- Bartus, R.T., Dean 3rd, R.L., Beer, B., Lippa, A.S., 1982. The cholinergic hypothesis of geriatric memory dysfunction. *Science* 217, 408–414.
- Baruch-Eliyahu, N., Rud, V., Braiman, A., Priel, E., 2019. Telomerase increasing compound protects hippocampal neurons from amyloid beta toxicity by enhancing the expression of neurotrophins and plasticity related genes. *Sci. Rep.* 9, 18118.
- Bellaver, B., Povala, G., Ferreira, P.C.L., Ferrari-Souza, J.P., Lefla, D.T., Lussier, F.Z., Benedet, A.L., Ashton, N.J., Triana-Baltzer, G., Kolb, H.C., Tissot, C., Theriault, J., Servaes, S., Stevenson, J., Rahmouni, N., Lopez, O.L., Tudorascu, D.L., Villemagne, V.L., Ikonomic, M.D., Gauthier, S., Zimmer, E.R., Zetterberg, H.,

- Blennow, K., Aizenstein, H.J., Klunk, W.E., Snitz, B.E., Maki, P., Thurston, R.C., Cohen, A.D., Ganguli, M., Karikari, T.K., Rosa-Neto, P., Pascoal, T.A., 2023. Astrocyte reactivity influences amyloid- β effects on tau pathology in preclinical Alzheimer's disease. *Nat. Med.* 29, 1775–1781.
- Brosseron, F., Krauthausen, M., Kummer, M., Heneka, M.T., 2014. Body fluid cytokine levels in mild cognitive impairment and Alzheimer's disease: a comparative overview. *Mol. Neurobiol.* 50, 534–544.
- Butterfield, D.A., Lange, M.L., 2009. Multifunctional roles of enolase in Alzheimer's disease brain: beyond altered glucose metabolism. *J. Neurochem.* 111, 915–933.
- Carter, S.F., Herholz, K., Rosa-Neto, P., Pellerin, L., Nordberg, A., Zimmer, E.R., 2019. Astrocyte biomarkers in Alzheimer's disease. *Trends Mol. Med.* 25, 77–95.
- Choi, J., Kim, H., Kim, Y., Jang, M., Jeon, J., Hwang, Y.I., Shon, W.J., Song, Y.W., Kang, J.S., Lee, W.J., 2015. The anti-inflammatory effect of GV1001 mediated by the downregulation of ENO1-induced pro-inflammatory cytokine production. *Immune Network* 15, 291–303.
- Cnops, V., Iyer, V.R., Parathy, N., Wong, P., Dawe, G.S., 2022. Test, rinse, repeat: A review of carryover effects in rodent behavioral assays. *Neurosci. Biobehav. Rev.* 135, 104560.
- Cummings, J., Lee, G., Nahed, P., Kambar, M., Zhong, K., Fonseca, J., Taghva, K., 2022. Alzheimer's disease drug development pipeline: 2022. *Alzheimers Dement. (N. Y.)* 8, e12295.
- D'Amico, A.V., Braccioforte, M.H., Moran, B.J., Chen, M.H., 2010. Luteinizing-hormone releasing hormone therapy and the risk of death from Alzheimer disease. *Alzheimer Dis. Assoc. Disord.* 24, 85–89.
- Dennison, J.L., Ricciardi, N.R., Lohse, I., Volmar, C.H., Wahlestedt, C., 2021. Sexual dimorphism in the 3xTg-AD mouse model and its impact on pre-clinical research. *J. Alzheimers Dis.* 80, 41–52.
- D'Hooge, R., De Deyn, P.P., 2001. Applications of the Morris water maze in the study of learning and memory. *Brain Res. Brain Res. Rev.* 36, 60–90.
- Di, L., 2015. Strategic approaches to optimizing peptide ADME properties. *AAPS J.* 17, 134–143.
- Frozza, R.L., Lourenco, M.V., De Felice, F.G., 2018. Challenges for Alzheimer's disease therapy: insights from novel mechanisms beyond memory defects. *Front. Neurosci.* 12, 37.
- Ghosh, M., Xu, Y., Pearse, D.D., 2016. Cyclic AMP is a key regulator of M1 to M2a phenotypic conversion of microglia in the presence of Th2 cytokines. *J. Neuroinflamm.* 13, 9.
- Goldberg, J., Currais, A., Prior, M., Fischer, W., Chiruta, C., Ratliff, E., Daugherty, D., Dargusch, R., Finley, K., Esparza-Moltó, P.B., Cuezva, J.M., Maher, P., Petrascheck, M., Schubert, D., 2018. The mitochondrial ATP synthase is a shared drug target for aging and dementia. *Aging Cell* 17.
- Grigорова, M., Sherwin, B.B., Tulandi, T., 2006. Effects of treatment with leuprolide acetate depot on working memory and executive functions in young premenopausal women. *Psychoneuroendocrinology* 31, 935–947.
- Grundtman, C., Kreutmayer, S.B., Almanzar, G., Wick, M.C., Wick, G., 2011. Heat shock protein 60 and immune inflammatory responses in atherosclerosis. *Arterioscler. Thromb. Vasc. Biol.* 31, 960–968.
- Hadas, S., Spira, M., Hanisch, U.K., Reichert, F., Rotshenker, S., 2012. Complement receptor-3 negatively regulates the phagocytosis of degenerated myelin through tyrosine kinase Syk and cofilin. *J. Neuroinflamm.* 9, 166.
- Haghani, A., Cacciottolo, M., Doty, K.R., D'Agostino, C., Thorwald, M., Safi, N., Levine, M.E., Sioutas, C., Town, T.C., Forman, H.J., Zhang, H., Morgan, T.E., Finch, C.E., 2020. Mouse brain transcriptome responses to inhaled nanoparticulate matter differed by sex and APOE in Nrf2-Nfkb interactions. *eLife* 9.
- He, Z., Guo, J.L., McBride, J.D., Narasimhan, S., Kim, H., Changolkar, L., Zhang, B., Gathagan, R.J., Yue, C., Dengler, C., Stieber, A., Nitla, M., Coulter, D.A., Abel, T., Brunten, K.R., Trojanowski, J.Q., Lee, V.M., 2018. Amyloid- β plaques enhance Alzheimer's brain tau-seeded pathologies by facilitating neuritic plaque tau aggregation. *Nat. Med.* 24, 29–38.
- Hughes, R.N., 2004. The value of spontaneous alternation behavior (SAB) as a test of retention in pharmacological investigations of memory. *Neurosci. Biobehav. Rev.* 28, 497–505.
- Jang, J.W., Park, J.H., Kim, S., Lee, S.H., Lee, S.H., Kim, Y.J., 2021. Prevalence and incidence of dementia in South Korea: a nationwide analysis of the national health insurance service senior cohort. *J. Clin. Neurol. (Seoul, Korea)* 17, 249–256.
- Javonillo, D.L., Tran, K.M., Phan, J., Hingco, E., Kramár, E.A., da Cunha, C., Forner, S., Kawauchi, S., Milinkeviciute, G., Gomez-Arboledas, A., Neumann, J., Banh, C.E., Huynh, M., Matheos, D.P., Rezaie, N., Alcantara, J.A., Mortazavi, A., Wood, M.A., Tenner, A.J., MacGregor, G.R., Green, K.N., LaFerla, F.M., 2021. Systematic phenotyping and characterization of the 3xTg-AD mouse model of Alzheimer's disease. *Front. Neurosci.* 15, 785276.
- Kim, W., Cho, S.B., Jung, H.Y., Yoo, D.Y., Oh, J.K., Choi, G.M., Cho, T.G., Kim, D.W., Hwang, I.K., Choi, S.Y., Moon, S.M., 2019b. Phosphatidylethanolamine-binding protein 1 ameliorates ischemia-induced inflammation and neuronal damage in the rabbit spinal cord. *Cells* 8.
- Kim, J.W., Yadav, D.K., Kim, S.J., Lee, M.Y., Park, J.M., Kim, B.S., Kim, M.H., Park, H.G., Kang, K.W., 2019a. Anti-cancer effect of GV1001 for prostate cancer: function as a ligand of GnRHR. *Endocr. Relat. Cancer* 26, 147–162.
- Kim, J.W., Park, M., Kim, S., Lim, S.C., Kim, H.S., Kang, K.W., 2021. Anti-metastatic effect of GV1001 on prostate cancer cells; roles of GnRHR-mediated Gas-cAMP pathway and AR-YAP1 axis. *Cell Biosci.* 11, 191.
- Ko, Y.J., Kwon, K.Y., Kum, K.Y., Lee, W.C., Baek, S.H., Kang, M.K., Shon, W.J., 2015. The anti-inflammatory effect of human telomerase-derived peptide on P. gingivalis lipopolysaccharide-induced inflammatory cytokine production and its mechanism in human dental pulp cells. *Mediat. Inflamm.* 2015, 385127.

- Koh, S.H., Kwon, H.S., Choi, S.H., Jeong, J.H., Na, H.R., Lee, C.N., Yang, Y., Lee, A.Y., Lee, J.H., Park, K.W., Han, H.J., Kim, B.C., Park, J.S., Lee, J.Y., Kim, S., Lee, K.Y., 2021. Efficacy and safety of GV1001 in patients with moderate-to-severe Alzheimer's disease already receiving donepezil: a phase 2 randomized, double-blind, placebo-controlled, multicenter clinical trial. *Alzheimers Res. Ther.* 13, 66.
- Krauter, A.K., Guest, P.C., Sarnyai, Z., 2019. The Y-maze for assessment of spatial working and reference memory in mice. *Methods Mol. Biol.* 1916, 105–111.
- Kwon, H.S., Koh, S.H., 2020. Neuroinflammation in neurodegenerative disorders: the roles of microglia and astrocytes. *Transl. Neurodegener.* 9, 42.
- Larkin, H.D., 2023. Lecanemab gains FDA approval for early Alzheimer disease. *JAMA* 329, 363.
- Lau, J.L., Dunn, M.K., 2018. Therapeutic peptides: Historical perspectives, current development trends, and future directions. *Bioorg. Med. Chem.* 26, 2700–2707.
- Liu, K.Y., Howard, R., 2021. Can we learn lessons from the FDA's approval of aducanumab? *Nature reviews. Neurology* 17, 715–722.
- Maeng, L.Y., Taha, M.B., Cover, K.K., Glynn, S.S., Murillo, M., Lebron-Milad, K., Milad, M.R., 2017. Acute gonadotropin-releasing hormone agonist treatment enhances extinction memory in male rats. *Psychoneuroendocrinology* 82, 164–172.
- Marbouti, L., Zahmatkesh, M., Riahi, E., Shafiee Sabet, M., 2020. GnRH protective effects against amyloid β -induced cognitive decline: A potential role of the 17 β -estradiol. *Mol. Cell. Endocrinol.* 518, 110985.
- Misrani, A., Tabassum, S., Huo, Q., Tabassum, S., Jiang, J., Ahmed, A., Chen, X., Zhou, J., Zhang, J., Liu, S., Feng, X., Long, C., Yang, L., 2021. Mitochondrial deficits with neural and social damage in early-stage Alzheimer's disease model mice. *Front. Aging Neurosci.* 13, 748388.
- Morris, R.G., Garrud, P., Rawlins, J.N., O'Keefe, J., 1982. Place navigation impaired in rats with hippocampal lesions. *Nature* 297, 681–683.
- Nazem, A., Sankowski, R., Bacher, M., Al-Abed, Y., 2015. Rodent models of neuroinflammation for Alzheimer's disease. *J. Neuroinflammation* 12, 74.
- Oakley, H., Cole, S.L., Logan, S., Maus, E., Shao, P., Craft, J., Guillozet-Bongaarts, A., Ohno, M., Disterhoft, J., Van Eldik, L., Berry, R., Vassar, R., 2006. Intraneuronal beta-amyloid aggregates, neurodegeneration, and neuron loss in transgenic mice with five familial Alzheimer's disease mutations: potential factors in amyloid plaque formation. *J. Neurosci.* 26, 10129–10140.
- Oksanen, M., Lehtonen, S., Jaronen, M., Goldsteins, G., Hämäläinen, R.H., Koistinaho, J., 2019. Astrocyte alterations in neurodegenerative pathologies and their modeling in human induced pluripotent stem cell platforms. *Cell. Mol. Life Sci.* 76, 2739–2760.
- Olfert, E., Bhasin, J., Latt, R., Macallum, E., McCutcheon, K., Rainnie, D., Schunk, M., 1998. The CCAC guidelines on: choosing an appropriate endpoint in experiments using animals for research. *Teaching and Testing Canadian Council on Animal Care guideline 1*, 1–30.
- Pardridge, W.M., 2020. Treatment of Alzheimer's disease and blood-brain barrier drug delivery. *Pharmaceuticals (Basel, Switzerland)* 13.
- Paris, D., Bachmeier, C., Patel, N., Quadros, A., Volmar, C.H., Laporte, V., Ganey, J., Beaulieu-Abdelahad, D., Ait-Ghezala, G., Crawford, F., Mullan, M.J., 2011. Selective antihypertensive dihydropyridines lower A β accumulation by targeting both the production and the clearance of A β across the blood-brain barrier. *Mol. Med. (Cambridge, Mass.)* 17, 149–162.
- Park, H.H., Lee, K.Y., Kim, S., Lee, J.W., Choi, N.Y., Lee, E.H., Lee, Y.J., Lee, S.H., Koh, S.H., 2014. Novel vaccine peptide GV1001 effectively blocks β -amyloid toxicity by mimicking the extra-telomeric functions of human telomerase reverse transcriptase. *Neurobiol. Aging* 35, 1255–1274.
- Park, H.H., Yu, H.J., Kim, S., Kim, G., Choi, N.Y., Lee, E.H., Lee, Y.J., Yoon, M.Y., Lee, K.Y., Koh, S.H., 2016. Neural stem cells injured by oxidative stress can be rejuvenated by GV1001, a novel peptide, through scavenging free radicals and enhancing survival signals. *Neurotoxicology* 55, 131–141.
- Park, H.H., Lee, K.Y., Park, D.W., Choi, N.Y., Lee, Y.J., Son, J.W., Kim, S., Moon, C., Kim, H.W., Rhyu, L.J., Koh, S.H., 2018. Tracking and protection of transplanted stem cells using a ferrocenecarboxylic acid-conjugated peptide that mimics hTERT. *Biomaterials* 155, 80–91.
- Prange-Kiel, J., Jarry, H., Schoen, M., Kohlmann, P., Lohse, C., Zhou, L., Rune, G.M., 2008. Gonadotropin-releasing hormone regulates spine density via its regulatory role in hippocampal estrogen synthesis. *J. Cell Biol.* 180, 417–426.
- Prince, M., Bryce, R., Albanese, E., Wimo, A., Ribeiro, W., Ferri, C.P., 2013. The global prevalence of dementia: a systematic review and metaanalysis. *Alzheimers Dement.* 9, 63–75.e62.
- Quintanar, J.L., Salinas, E., 2008. Neurotrophic effects of GnRH on neurite outgrowth and neurofilament protein expression in cultured cerebral cortical neurons of rat embryos. *Neurochem. Res.* 33, 1051–1056.
- Relitti, N., Saraswati, A.P., Federico, S., Khan, T., Brindisi, M., Zisterer, D., Brogi, S., Gemma, S., Butini, S., Campiani, G., 2020. Telomerase-based cancer therapeutics: a review on their clinical trials. *Curr. Top. Med. Chem.* 20, 433–457.
- Schott, J.M., Aisen, P.S., Cummings, J.L., Howard, R.J., Fox, N.C., 2019. Unsuccessful trials of therapies for Alzheimer's disease. *Lancet* 393, 29.
- Skinner, D.C., Malpau, B., Delaleu, B., Caraty, A., 1995. Luteinizing hormone (LH)-releasing hormone in third ventricular cerebrospinal fluid of the ewe: correlation with LH pulses and the LH surge. *Endocrinology* 136, 3230–3237.
- Takata, K., Kitamura, Y., Saeki, M., Terada, M., Kagitani, S., Kitamura, R., Fujikawa, Y., Maelicke, A., Tomimoto, H., Taniguchi, T., Shimohama, S., 2010. Galantamine-induced amyloid- β clearance mediated via stimulation of microglial nicotinic acetylcholine receptors. *J. Biol. Chem.* 285, 40180–40191.
- Tang, Y., Le, W., 2016. Differential roles of M1 and M2 microglia in neurodegenerative diseases. *Mol. Neurobiol.* 53, 1181–1194.
- Ullman-Cullere, M.H., Foltz, C.J., 1999. Body condition scoring: a rapid and accurate method for assessing health status in mice. *Lab Anim Sci* 49, 319–323.
- Wang, F., Zhang, Z., Han, J., Zheng, J., Wang, X., Wang, Z., 2023. Discovery of microglia gonadotropin-releasing hormone receptor and its potential role in polycystic ovarian syndrome. *Mol. Med. Reports* 27.
- Wang, Q., Yuan, W., Yang, X., Wang, Y., Li, Y., Qiao, H., 2020. Role of cofilin in Alzheimer's disease. *Front. Cell Dev. Biol.* 8, 584898.
- Xu, Y., Li, W., Shi, M., Xu, X., Guo, D., Liu, Z., Chen, L., Zhong, X., Cao, W., 2023. Systemic treatment with GnRH agonist produces antidepressant-like effects in LPS induced depression male mouse model. *Neuropharmacology* 233, 109560.
- Zhang, G., Li, J., Purkayastha, S., Tang, Y., Zhang, H., Yin, Y., Li, B., Liu, G., Cai, D., 2013. Hypothalamic programming of systemic ageing involving IKK- β , NF- κ B and GnRH. *Nature* 497, 211–216.